

A bulky and stable copper(I)-phenanthroline complex: impact of steric strain and symmetry on the excited-state properties.

Lea Gimeno,¹ Brian T. Phelan,² Emily A. Sprague-Klein,² Thierry Roisnel,³ Errol Blart,¹ Christophe Gourlaouen,^{4*} Lin X. Chen,^{2,5*} Yann Pellegrin^{1*}

¹Université de Nantes, CNRS, CEISAM UMR6230, F-44000 Nantes, France

²Chemical Science and Engineering Division, Argonne National Laboratory, Lemont, Illinois 60439, United States

³Université de Rennes CNRS, Institut des Sciences Chimiques de Rennes, UMR6226, F-35000 Rennes, France

⁴Laboratoire de Chimie Quantique Institut de Chimie UMR 7177 CNRS-Université de Strasbourg, 4, Rue Blaise Pascal CS 90032, F-67081 Strasbourg Cedex, France

⁵Department of Chemistry, Northwestern University, Evanston Illinois 60208, United States

Corresponding authors Email addresses:

gourlaouen@unistra.fr

lchen@anl.gov

Yann.pellegrin@univ-nantes.fr

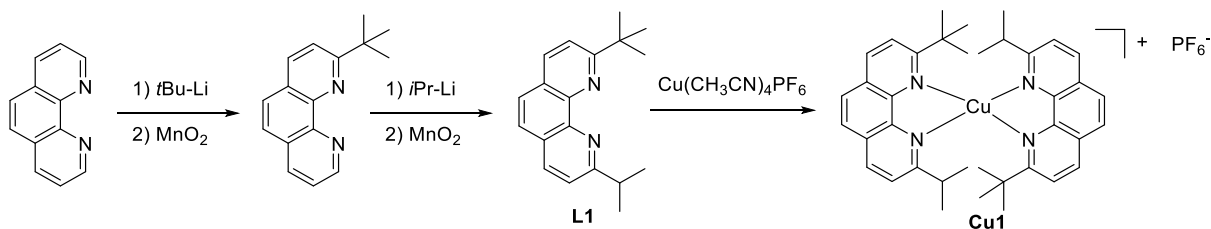


Figure S1. Synthesis of ligand L1 and complex Cu1.

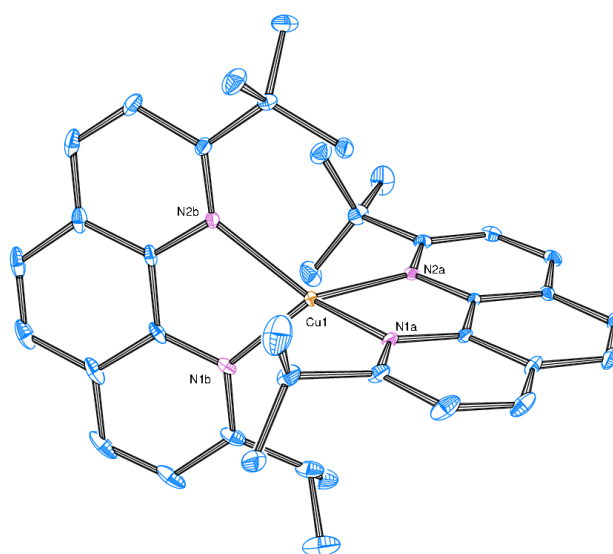


Figure S2. ORTEP view of complex **Cu1**. Ellipsoids are drawn at 50% probability level. Counter-anion omitted for clarity

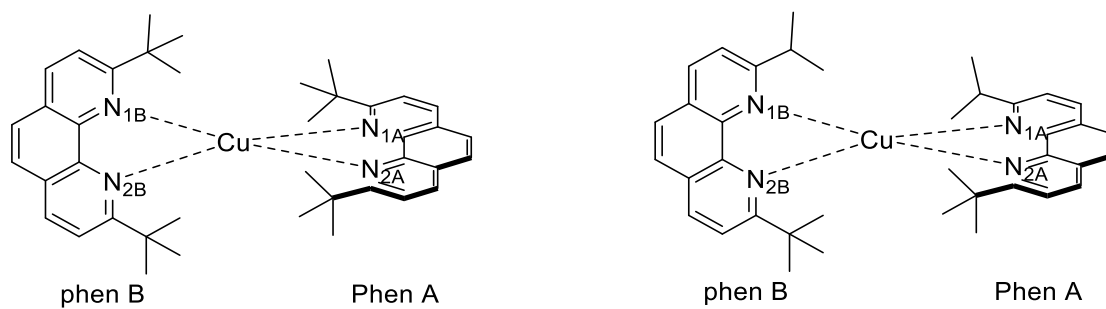


Figure S3. Used nomenclature to name nitrogen atoms with regards to the position of isopropyl or *tert*-butyl bulky groups.

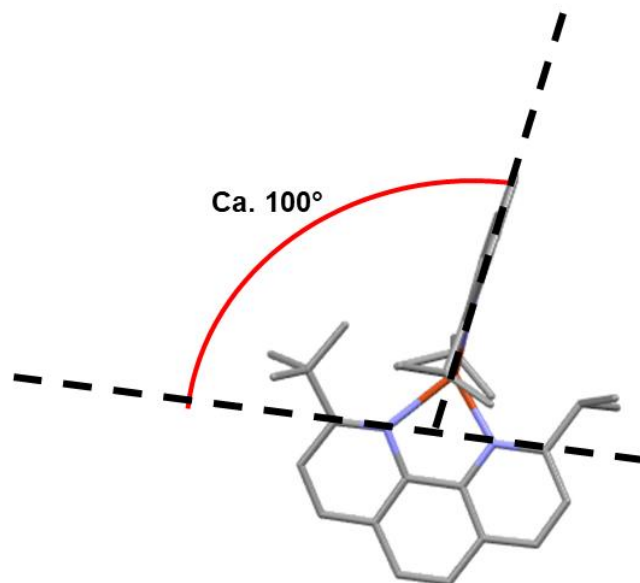


Figure S4. Illustration of the steric repulsion induced by *tert*-butyl vs. isopropyl substituents.

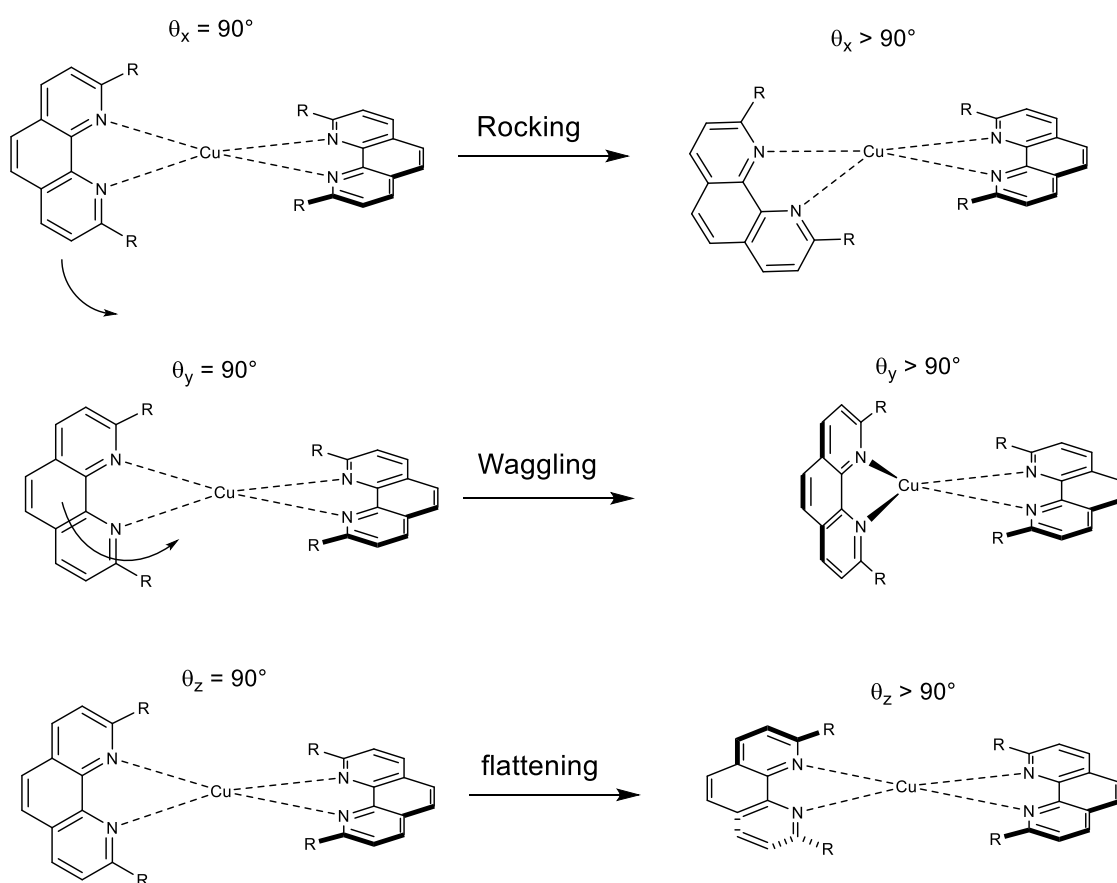


Figure S5. Illustration of the various distortion motions in homoleptic copper(I) complexes, related to θ_x , θ_y and θ_z angles.

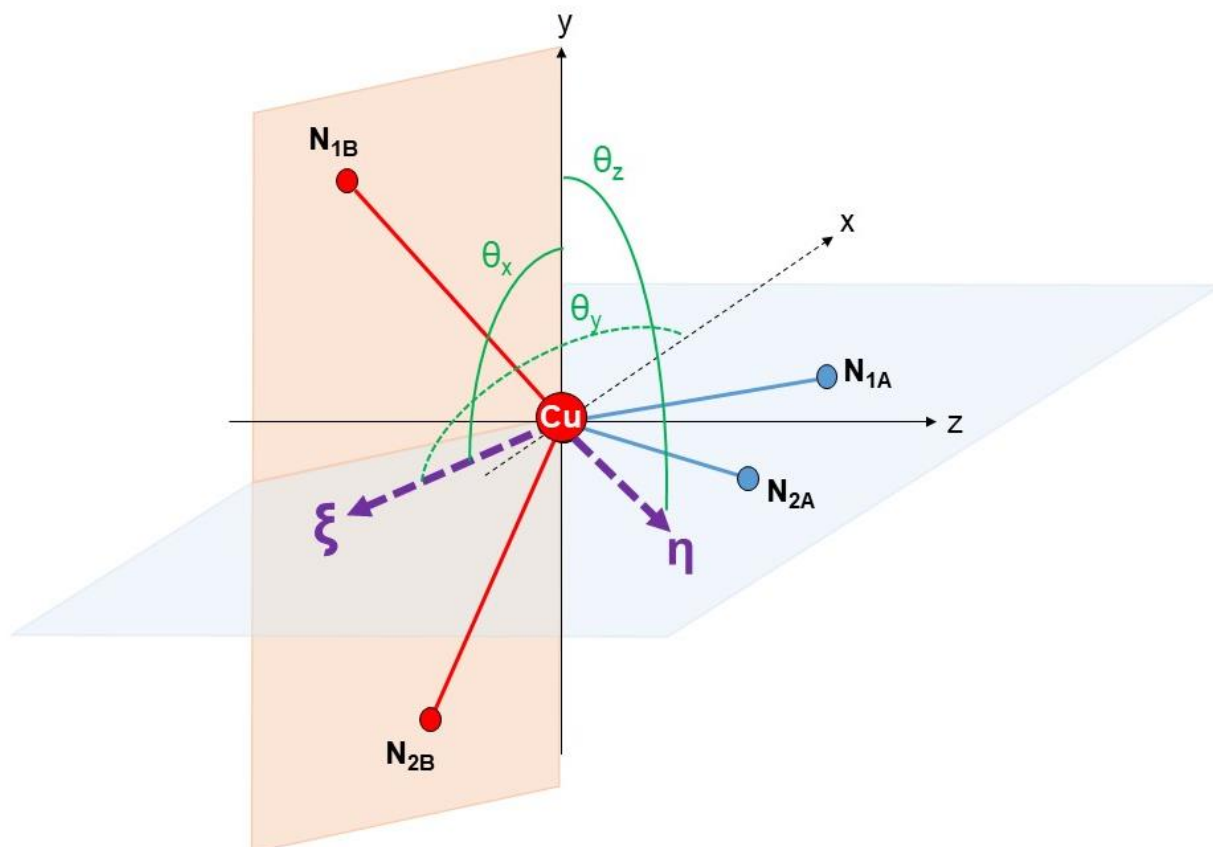


Figure S6. Illustration of the $\theta_{x,y,z}$ angles and the parameters necessary to define and measure them. Phenanthroline A is in the (x,z) plane, unit vector ξ is bisecting angle N_{1B} -Cu- N_{2B} , unit vector η is orthogonal to the plane defined by Cu, N_{1B} and N_{2B} , θ_x is the angle between ξ and y, θ_y is the angle between ξ and x and θ_z is the angle between y and η . $\theta_{x,y,z}$ angles have been calculated according to the protocol described in the literature.¹

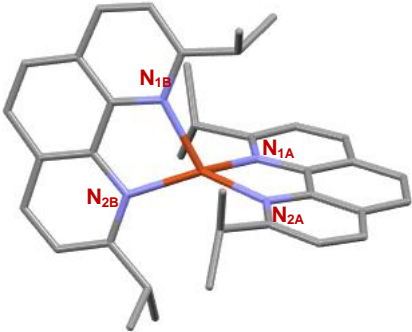
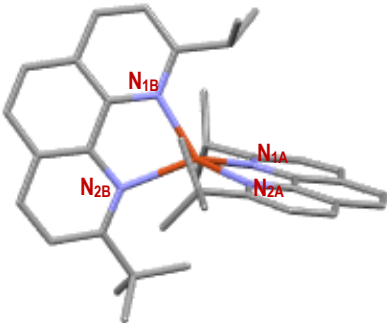
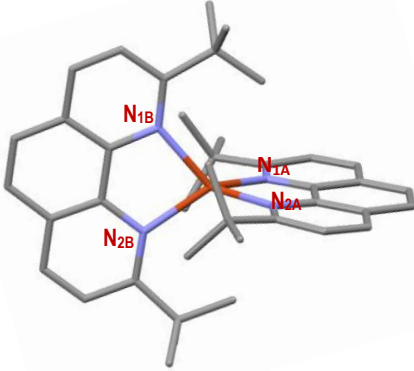
Complex	structure
<p data-bbox="379 293 568 322">[Cu(dipp)₂]⁺ [2]</p> <p data-bbox="379 394 501 423">$\theta_x = 82.2$</p> <p data-bbox="379 427 501 456">$\theta_y = 72.5$</p> <p data-bbox="379 461 501 490">$\theta_z = 85.4$</p>	
<p data-bbox="379 674 437 703">Cu1</p> <p data-bbox="379 775 501 804">$\theta_x = 87.2$</p> <p data-bbox="379 808 501 837">$\theta_y = 87.4$</p> <p data-bbox="379 842 501 871">$\theta_z = 87.3$</p>	
<p data-bbox="379 1099 544 1167">[Cu(dtbp)₂]⁺, (BF₄⁻)^[3]</p> <p data-bbox="379 1238 501 1267">$\theta_x = 88.6$</p> <p data-bbox="379 1272 501 1301">$\theta_y = 90.0$</p> <p data-bbox="379 1305 501 1335">$\theta_z = 91.8$</p>	

Figure S7. Structures and spatial disposition for the calculations of $\theta_{x,y,z}$ angles. Hydrogen atoms, solvent molecules and counter anions have been omitted for clarity.

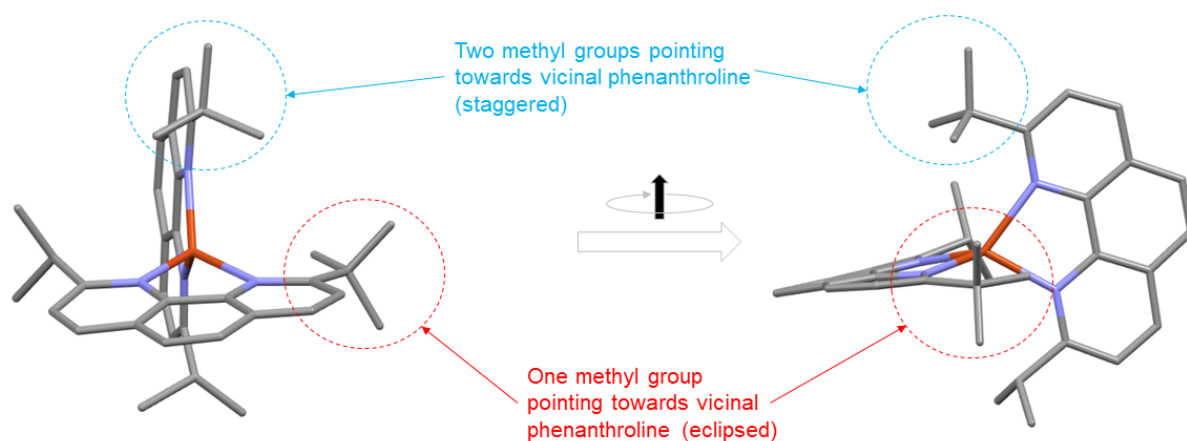


Figure S8. Illustration of the two different conformations of the *t*Bu groups in the structure of **Cu1** (the structures of the left and on the right are two different views of the same structure obtained by rotation along a vertical axis).

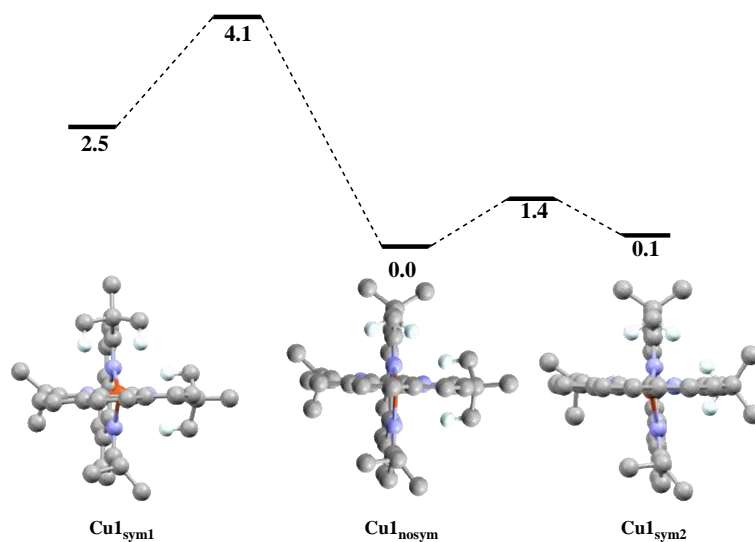


Figure S9. Reaction pathway for *tert*-Butyl rotation, energies are in kcal/mol.

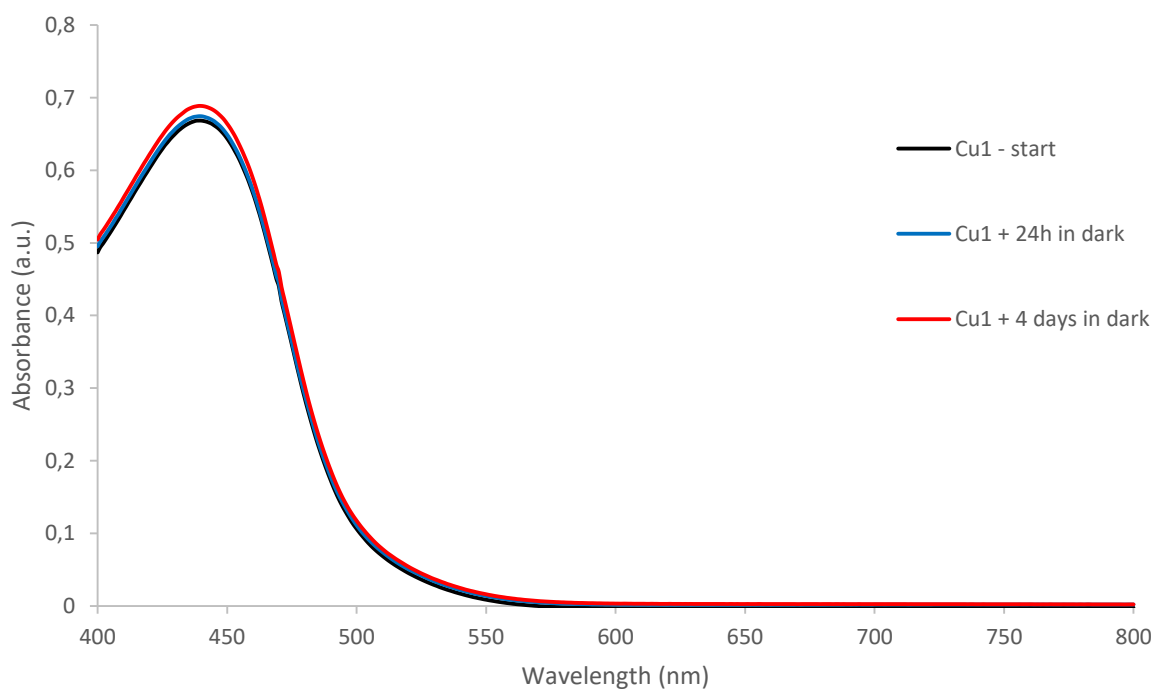
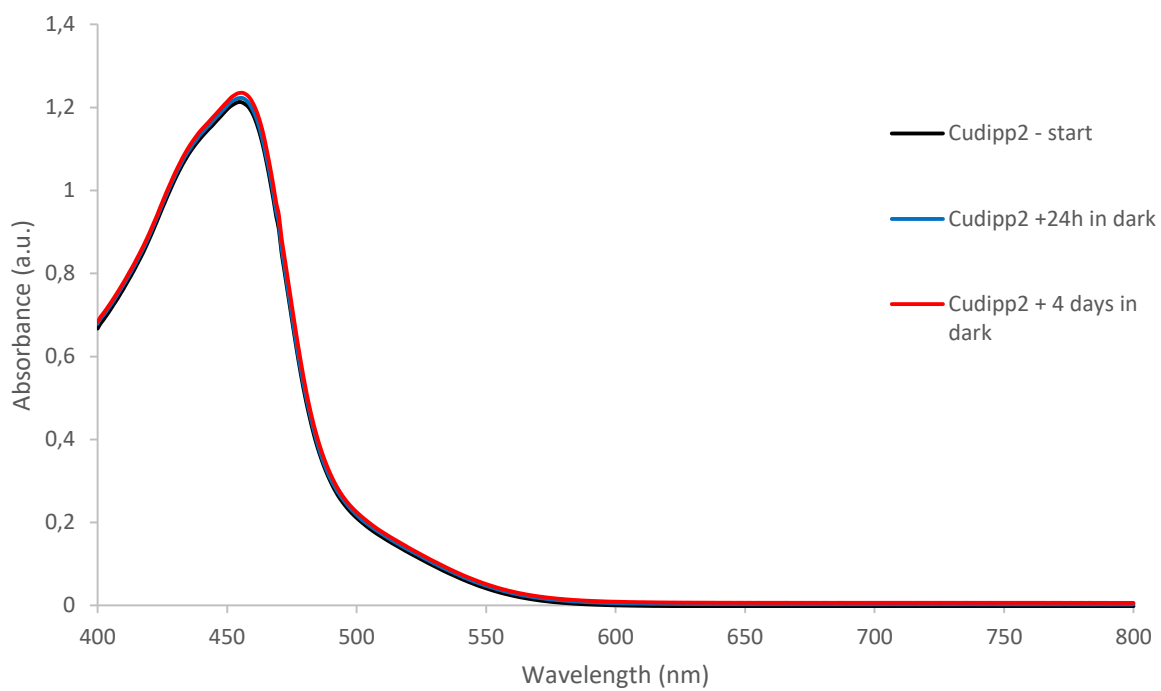


Figure S10. Evolution of the UV-Vis spectra of $[\text{Cu}(\text{dipp})_2]^+$ (up) and **Cu1** (bottom) in dichloromethane when shelved in ambient conditions (dotted lines) or when stored in dark (plain lines).

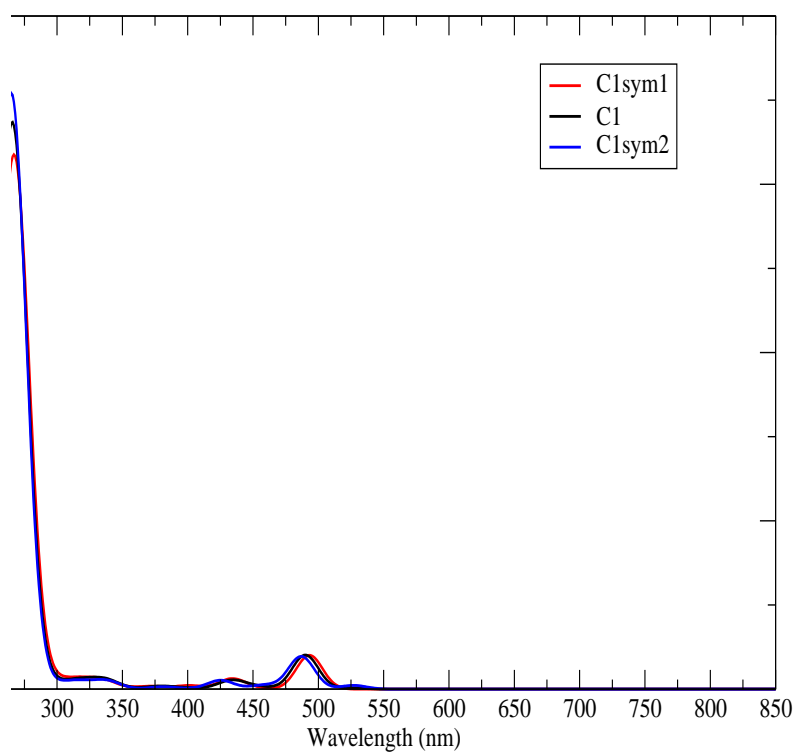


Figure S11. Overlaid absorption spectra of the three rotamers of **Cu1**.

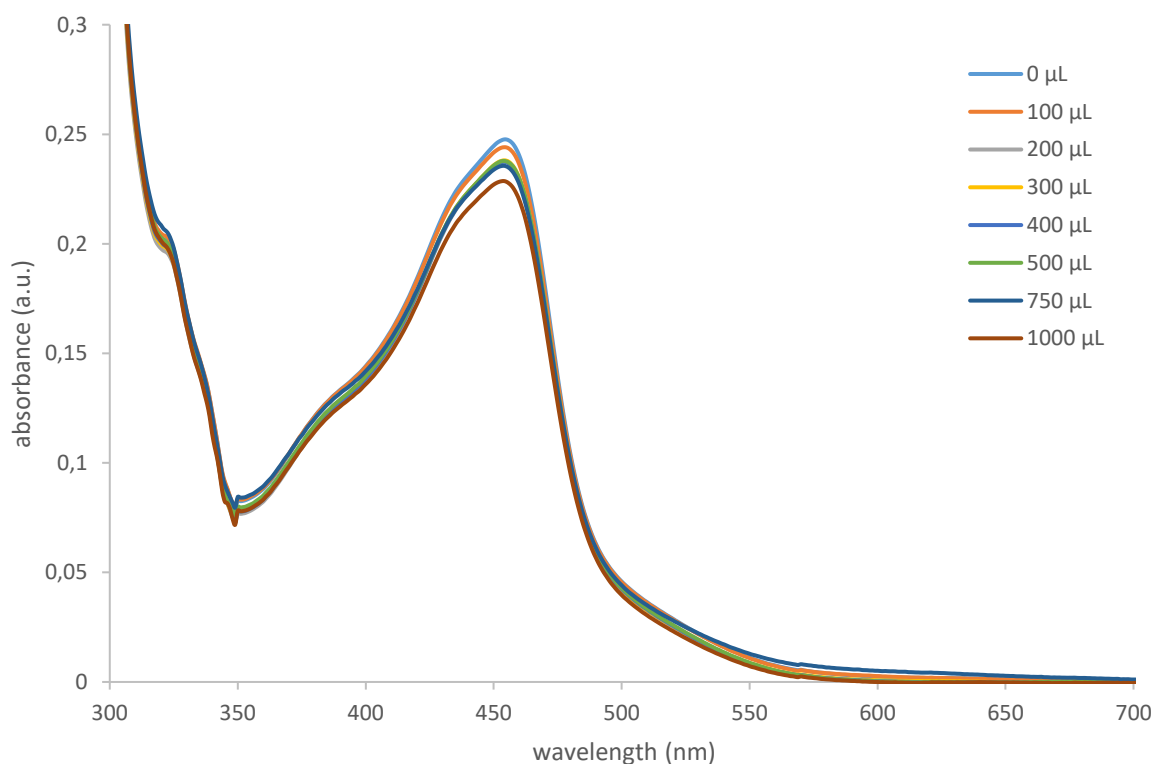
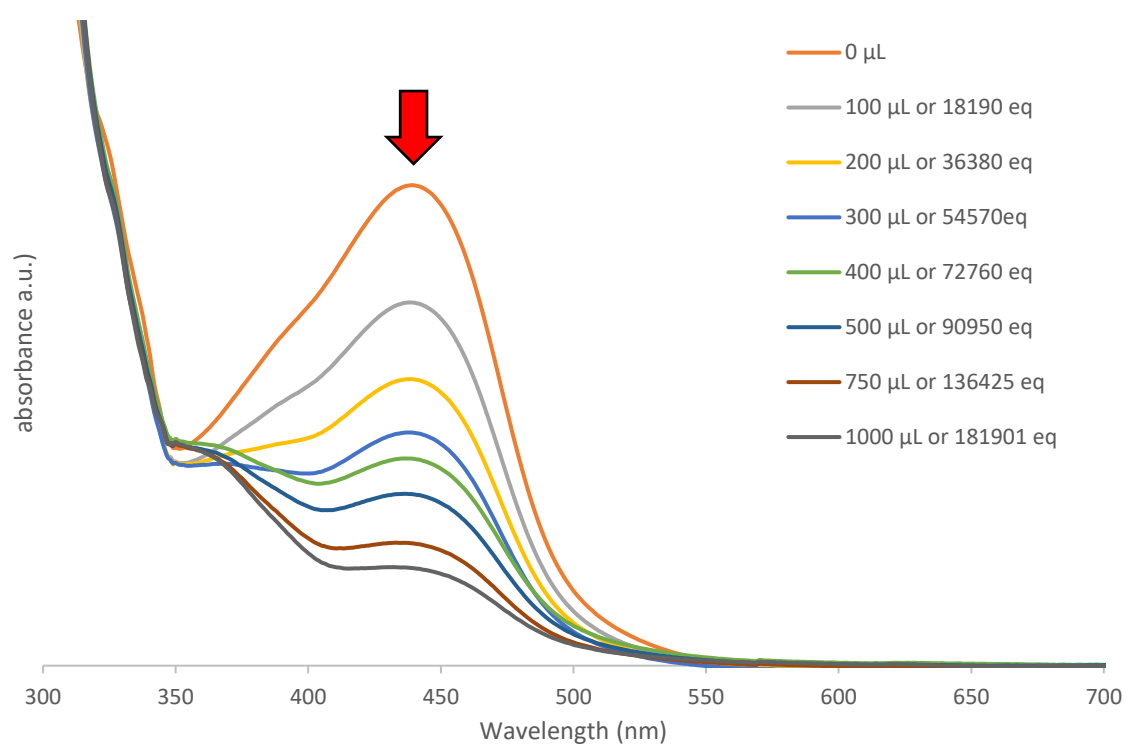


Figure S12. Evolution of the absorption spectra of **Cu1** (up) and [Cu(dipp)₂]⁺ (bottom) in dichloromethane upon addition of controlled aliquots of acetonitrile (normalized vs. dilution).

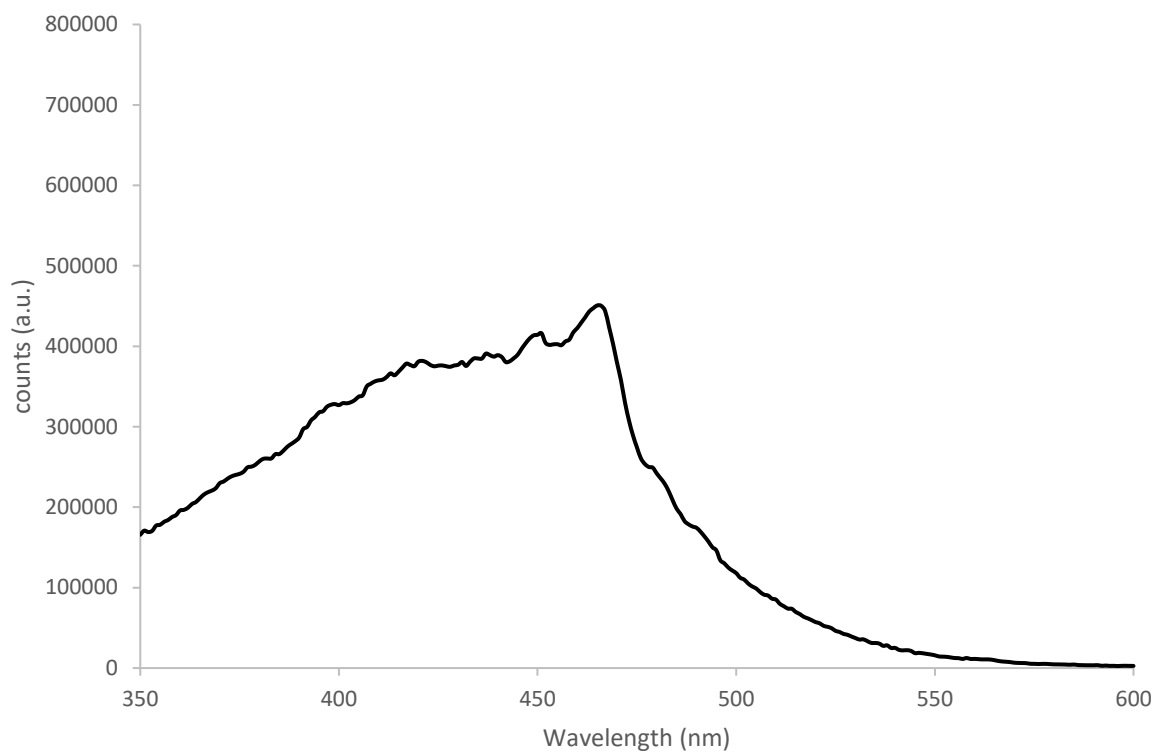


Figure S13. Excitation spectrum of **Cu1** in dichloromethane ($\lambda_{em} = 678$ nm).

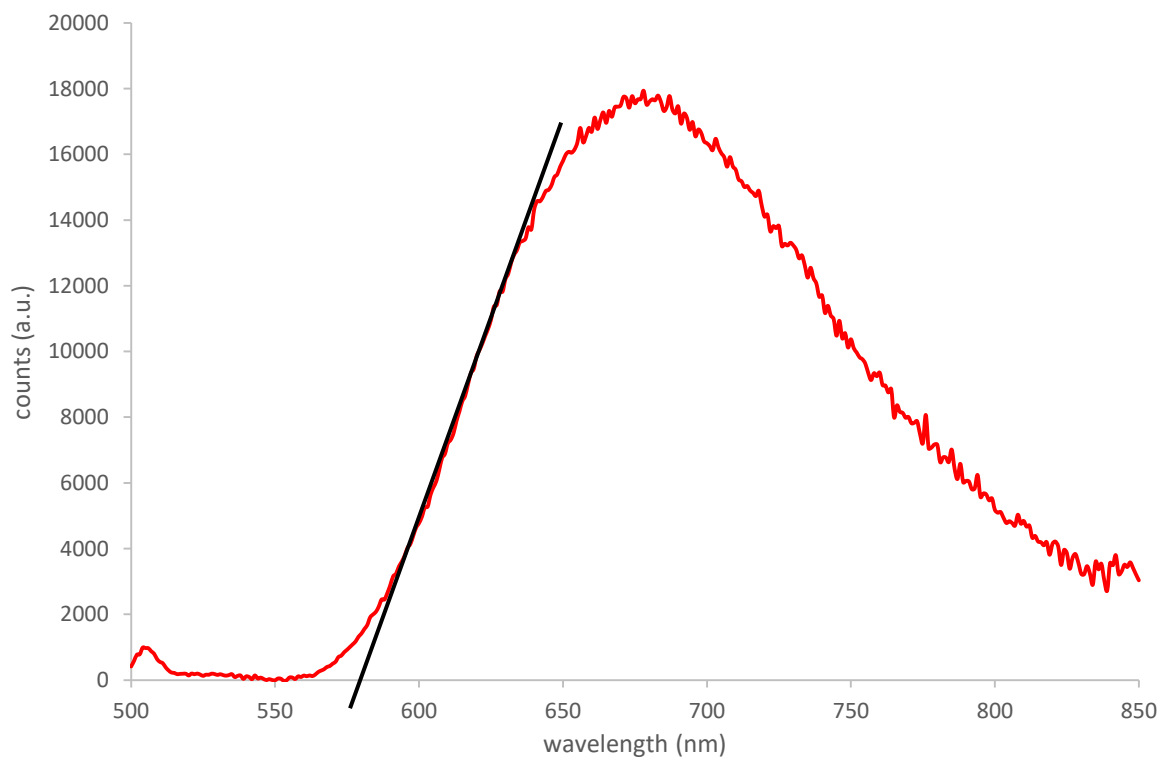


Figure S14. Determination of E^0 for **Cu1** by the tangent method.

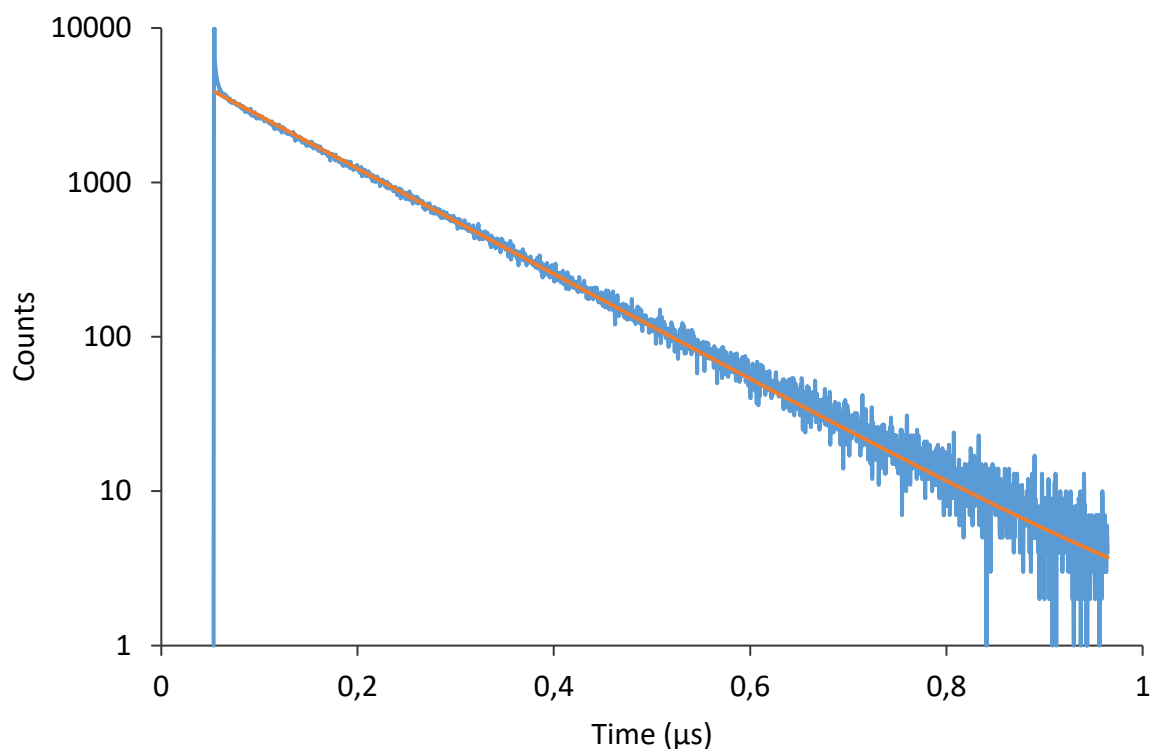


Figure S15. Decay of the emission intensity vs. time recorded by time correlated single photon counting for complex **Cu1** in degassed dichloromethane solution. Blue line: experimental data. Orange solid line: fitting of the long-lived decay.

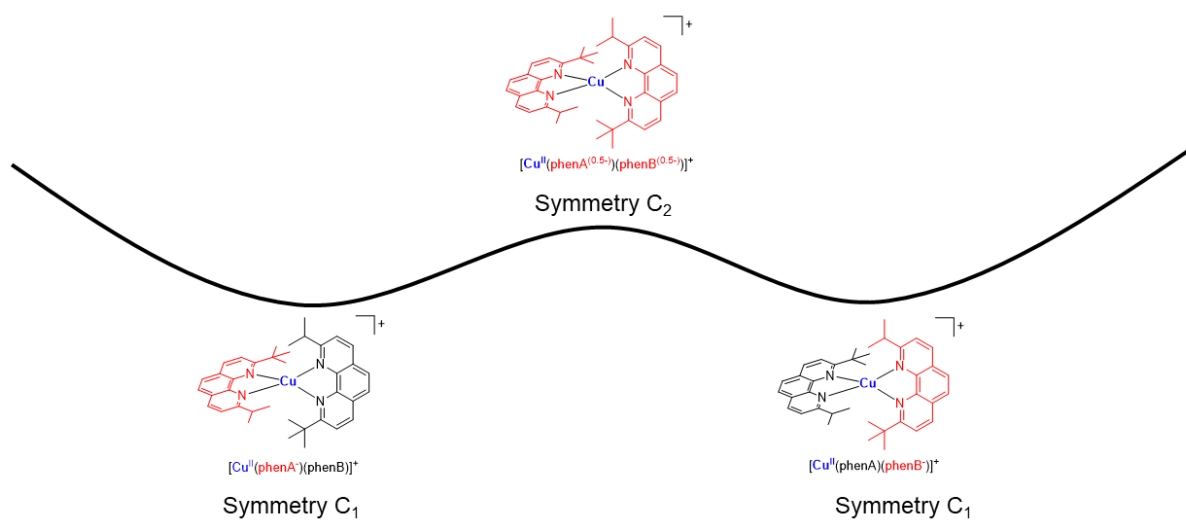


Figure S16. Illustration of the symmetry of the excited state whether the electron is localized on one ligand or on both. In red is symbolized the electron density localization, in blue the electron density depletion. The illustration is the same for **Cu1_{sym1}** and **Cu1_{sym2}**. For **Cu1_{nosym}**, one must bear in mind that when the electron is delocalized over the two ligands, the symmetry remains C₁ because of the symmetry constraints imposed by the different orientations of the *tert*-butyl groups.

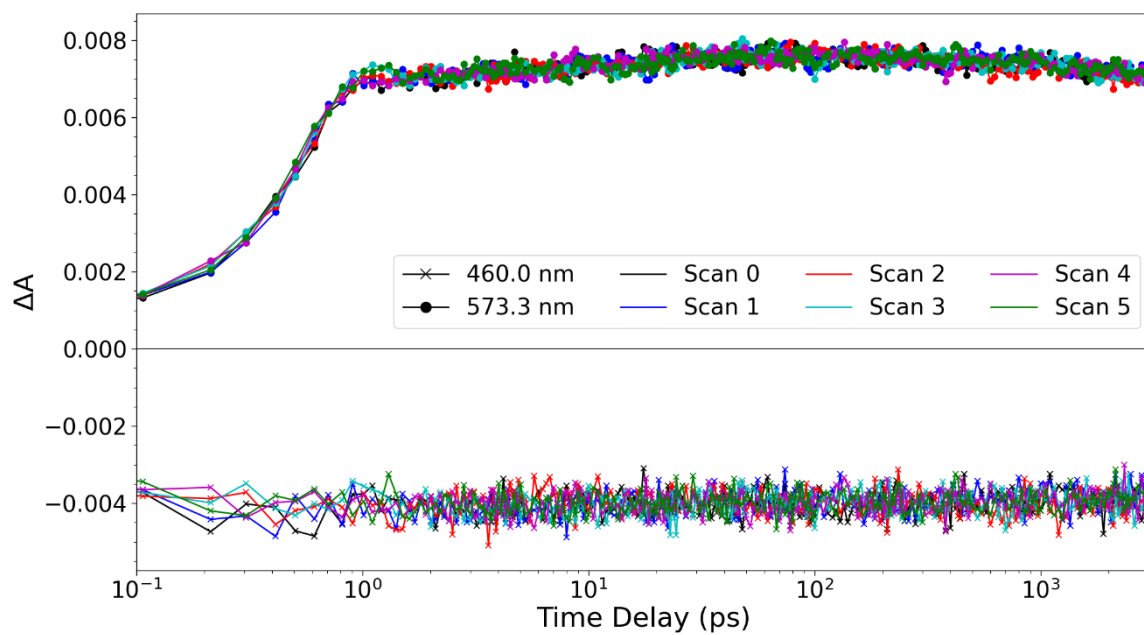


Figure S17. Overlay of the transient signals at the peak of the ground-state bleach (460.0 nm) and excited-state absorption (573.3 nm) from sequential scans of the optical delay stage showing no change in signal over the course of the 30 min transient absorption measurement. The pump pulse was centered at 415 nm with 500 nJ/pulse (0.25 mW at 0.5 kHz) and was focused to about 300 μm at the sample.

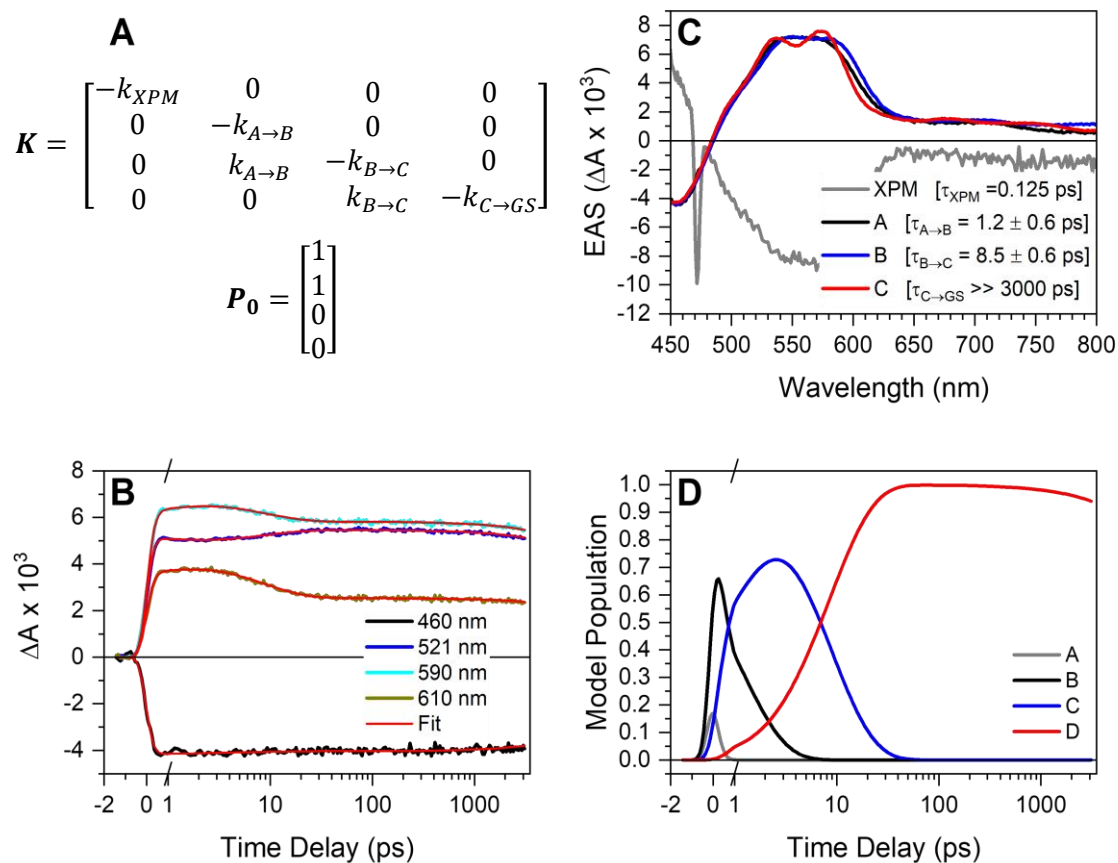


Figure S18. (A) Rate matrix K and initial population matrix P_0 used in first-order sequential kinetic model. XPM stands for cross-phase modulation and captures the coherent signals that occur when the pump and probe laser pulses are overlapped in time. (B) Kinetic traces at select probe wavelengths overlaid with the kinetic fit. (C) Evolution-associated spectra for each state in the kinetic model and (D) the model population traces for each state in the kinetic model.

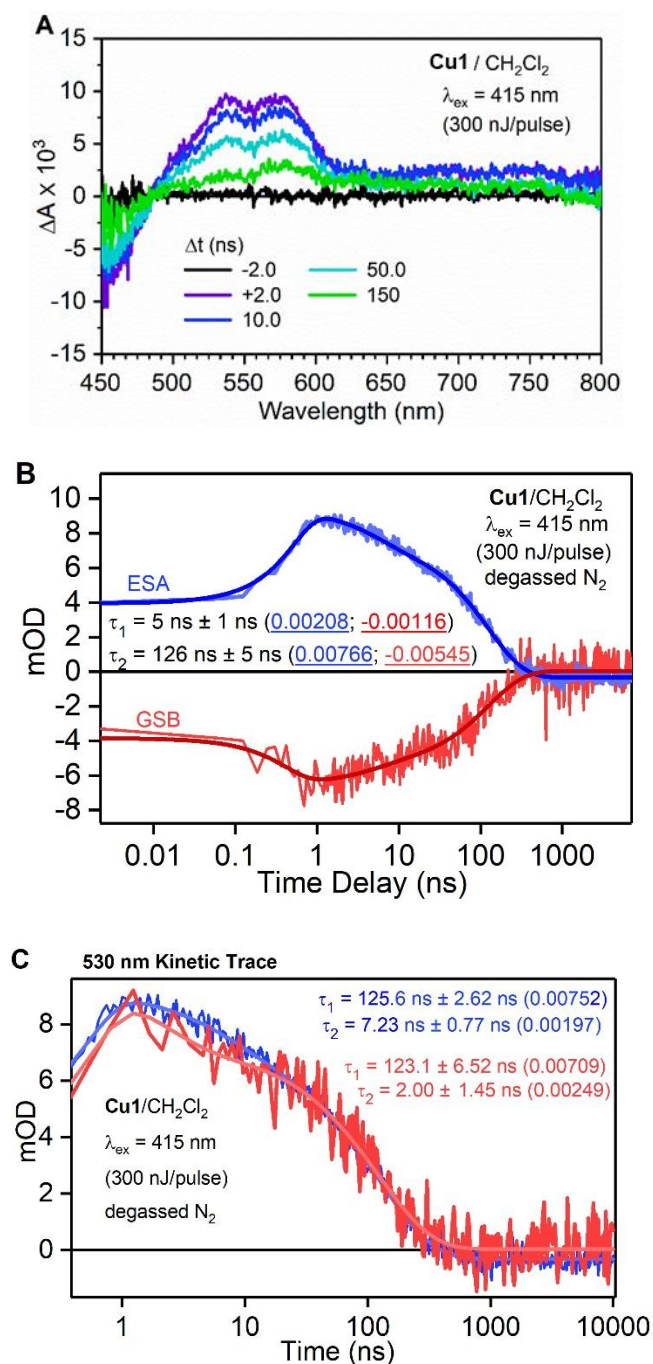


Figure S19. (A) Optical transient absorption spectra at nanosecond through microsecond time delays following excitation by 415 nm laser pulses for a solution of **Cu1** in dichloromethane. (B) Global fit of kinetic traces at probe wavelengths corresponding to the ESA and GSB with shared decay lifetimes τ_1 and τ_2 . The corresponding amplitudes for the ESA and GSB are shown in blue and red, respectively. (C) Overlaid kinetic traces from two separate experimental trials of **Cu1** in dichloromethane showing the biexponential dynamics. The two kinetic traces were fit independently and show similar values and relative amplitudes for τ_1 and τ_2 .

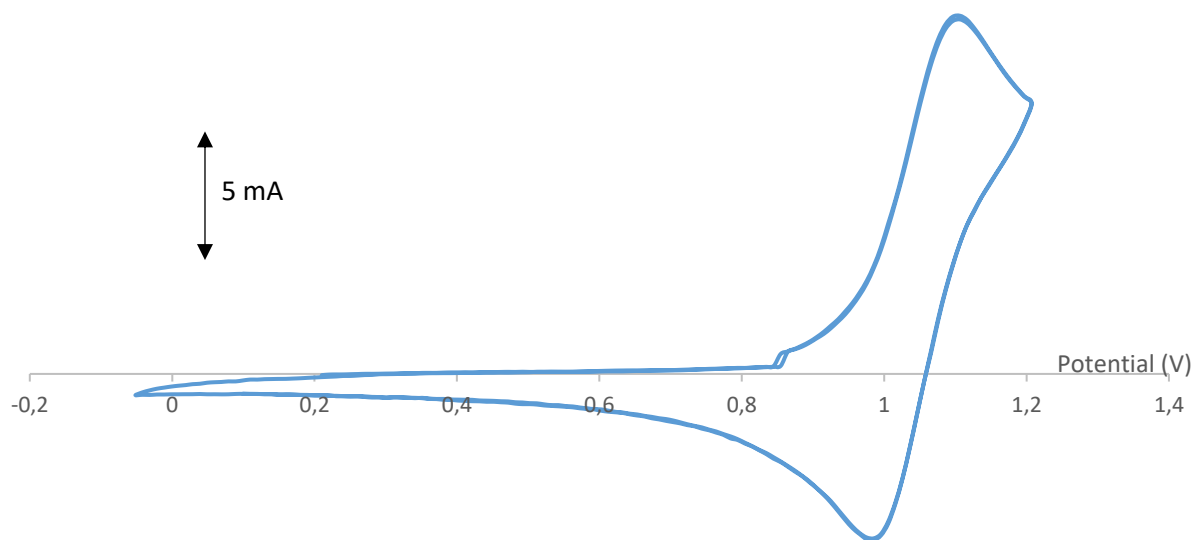


Figure S20. Cyclic voltammograms for complexes **Cu1** ($\text{Cu}^{\text{II}}/\text{Cu}^{\text{I}}$ couple) in argon purged dichloromethane. The working electrode is a platinum disk (2 mm diameter), the counter-electrode is a platinum sheet (ca 0.25 cm²) and the reference electrode is the saturated calomel electrode (SCE). There is no signal below -0.1 V vs. SCE within the solvent activity window. All potentials in the main text are referred to the ferrocinium/ferrocene couple which was added at the end of each experiment.

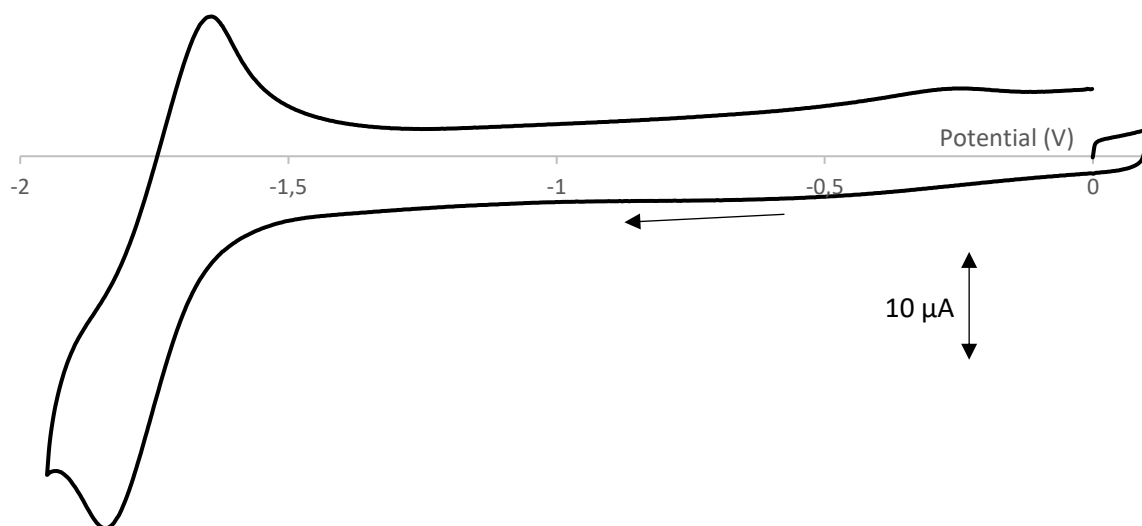
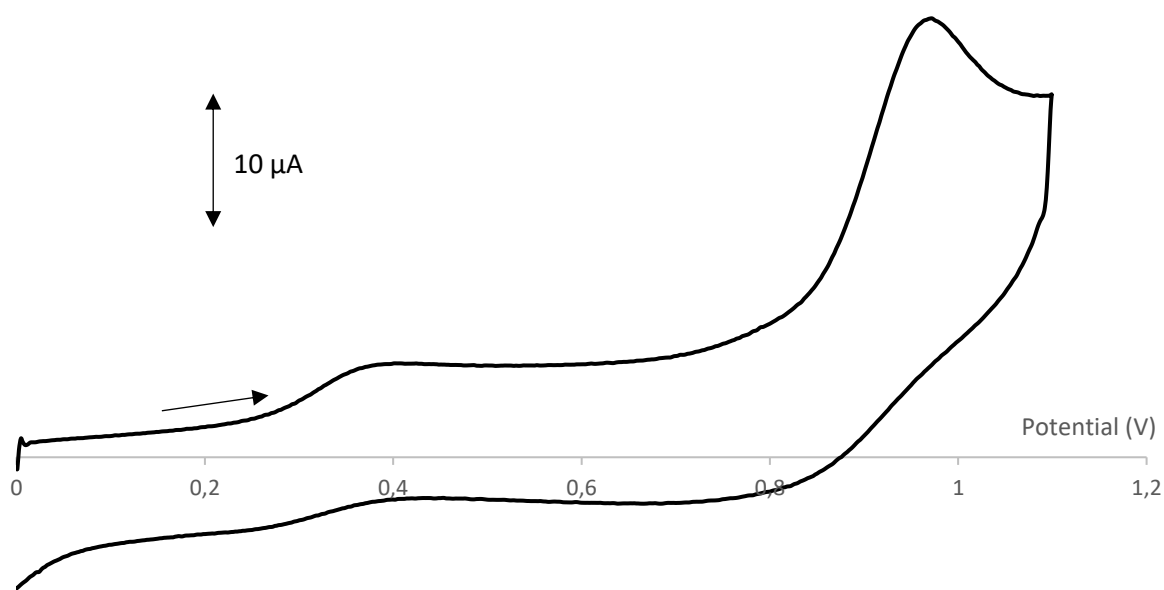


Figure S21. Cyclic voltammograms for complexes **Cu1** (addition of an extra electron on a coordinated ligand) in argon purged dimethylformamide. The working electrode is a platinum disk (2mm diameter), the counter-electrode is a platinum sheet (0.25 cm²) and the reference electrode is a silver/silver nitrate reference. All potentials in the main text are referred to the ferrocinium/ferrocene couple which was added at the end of each experiment.

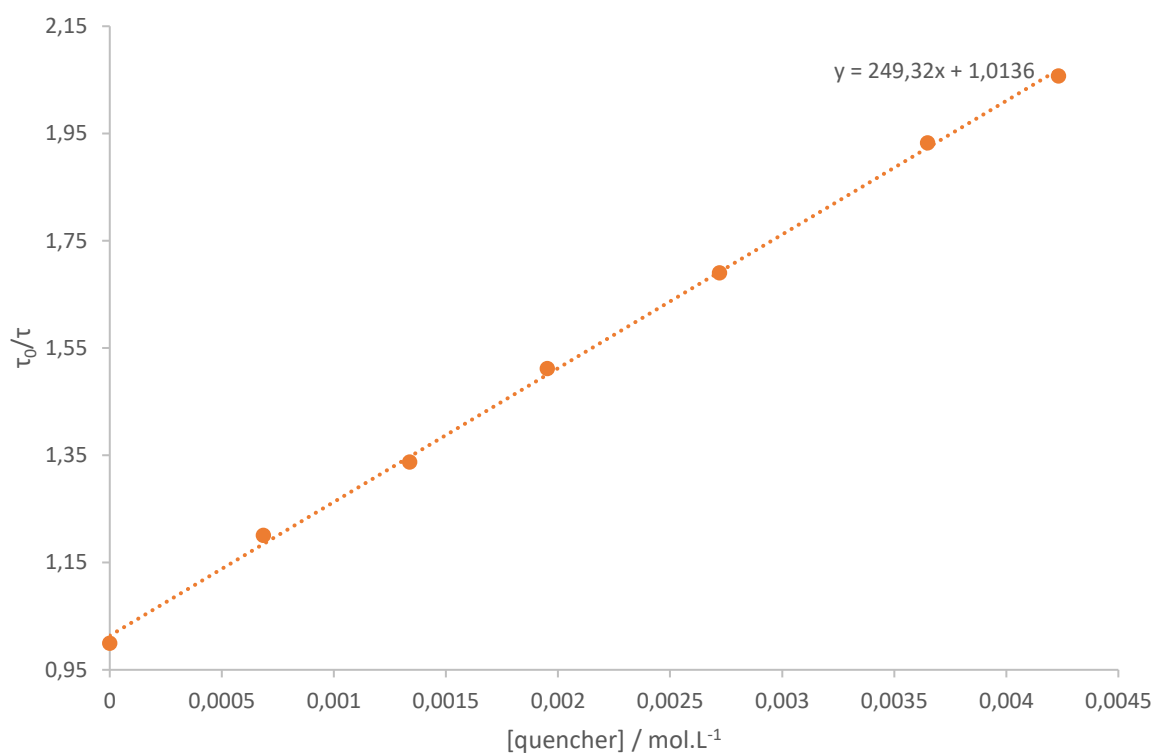


Figure S22. Stern-Volmer plots: monitoring the quenching of the luminescence of complex **Cu1** in presence of decamethylferrocene (dmFc, orange line).

Table ST1. Bond lengths (in Å) and angles (in degrees) of interest for the three rotamers of **Cu1** computed with ADF (ground state) in C_1 point group.

	Cu1sym1	Cu1nosym	Cu1sym2
Cu-N1B	2.052	2.051	2.015
Cu-N1A	2.052	2.026	2.015
Cu-N2B	2.122	2.132	2.199
Cu-N2A	2.122	2.179	2.199
N1B-Cu-N2B	83.14	82.51	82.05
N1B-Cu-N1A	110.38	114.88	123.46
N1B-Cu-N2A	121.84	119.35	120.3
N2B-Cu-N1A	121.84	121.99	120.3
N2B-Cu-N2A	138.11	138.8	134.51
N1A-Cu-N2A	83.14	82.36	82.05
X-Cu-X	163.0	160.4	162.7
$C\alpha$ -X-X- $C\alpha$	83.7	89.9	97.3
τ_4	0.71	0.70	0.72

Table ST2. Energy (in Ev), wavelength (nm), oscillator strength and nature of the singlet states of the absorption spectrum of **Cu1**.

State	Energy	Wavelength	Oscillator	MC	LC	MLCT	LMCT	LLCT
1	2.359	525	8.00E-03	2.29%	18.81%	71.27%	0.81%	6.82%
2	2.420	512	1.00E-03	2.20%	19.00%	71.25%	0.79%	6.75%
3	2.530	490	2.03E-01	2.20%	8.19%	72.61%	0.70%	16.30%
4	2.707	458	7.00E-03	0.48%	17.50%	72.27%	0.17%	9.58%
5	2.728	454	4.00E-03	0.12%	18.75%	72.58%	0.04%	8.52%
6	2.816	440	2.10E-02	1.11%	6.63%	74.93%	0.34%	17.00%
7	2.862	433	1.30E-02	1.28%	8.49%	74.54%	0.38%	15.31%
8	2.880	430	2.60E-02	0.10%	9.05%	74.06%	0.04%	16.76%
9	3.084	402	6.00E-03	2.70%	5.35%	86.20%	0.33%	5.42%
10	3.146	394	2.00E-03	2.59%	5.22%	85.49%	0.33%	6.37%
11	3.237	383	2.00E-03	3.35%	3.87%	89.09%	0.25%	3.45%
12	3.258	381	1.20E-02	3.39%	4.45%	88.06%	0.28%	3.83%
13	3.333	372	3.00E-03	3.20%	2.98%	90.57%	0.20%	3.05%
14	3.354	370	3.00E-03	2.56%	6.53%	85.17%	0.28%	5.47%
15	3.462	358	1.00E-03	0.49%	6.00%	87.57%	0.07%	5.87%
16	3.498	354	1.00E-03	0.06%	6.14%	87.92%	0.01%	5.87%
17	3.658	339	3.50E-02	0.08%	8.87%	85.90%	0.07%	5.09%
18	3.692	336	1.00E-02	0.52%	6.07%	87.33%	0.09%	5.99%
19	3.702	335	1.00E-03	0.55%	5.53%	87.88%	0.09%	5.96%
20	3.725	333	3.00E-03	0.43%	7.72%	86.28%	0.14%	5.42%
21	3.755	330	1.00E-02	1.03%	13.42%	77.53%	0.32%	7.69%
22	3.800	326	2.00E-03	1.06%	17.90%	73.81%	0.36%	6.88%
23	3.896	318	4.10E-02	1.12%	12.65%	70.28%	0.36%	15.60%
24	3.992	311	4.00E-03	0.67%	71.15%	19.75%	1.68%	6.75%
25	4.038	307	1.40E-02	0.11%	80.25%	10.00%	1.97%	7.67%
26	4.150	299	2.00E-03	0.91%	25.29%	48.33%	1.29%	24.18%
27	4.173	297	1.00E-03	0.25%	5.36%	11.74%	2.49%	80.17%
28	4.177	297	1.00E-03	0.10%	7.06%	2.81%	2.67%	87.36%
29	4.244	292	2.70E-02	0.05%	90.08%	3.94%	1.23%	4.71%
30	4.261	291	9.00E-03	0.07%	89.63%	5.18%	1.28%	3.84%
31	4.385	283	2.00E-03	0.80%	18.17%	68.74%	0.35%	11.95%
32	4.414	281	2.00E-03	0.01%	3.04%	3.27%	0.39%	93.29%
33	4.420	281	5.00E-03	0.01%	2.94%	3.36%	0.28%	93.42%
34	4.437	279	1.00E-03	0.22%	18.66%	71.83%	0.10%	9.20%
35	4.461	278	1.90E-02	0.05%	3.29%	1.83%	2.72%	92.12%
36	4.501	275	7.00E-03	0.82%	11.95%	68.37%	0.48%	18.38%
37	4.512	275	1.50E-02	1.28%	7.48%	81.58%	0.24%	9.43%
38	4.523	274	5.20E-02	0.17%	5.59%	7.03%	2.53%	84.70%
39	4.552	272	1.50E-02	1.22%	7.79%	82.88%	0.24%	7.88%
40	4.558	272	3.70E-02	0.15%	16.93%	69.19%	0.21%	13.52%
41	4.574	271	7.22E-01	0.49%	60.06%	33.79%	1.53%	4.13%
42	4.587	270	7.07E-01	0.46%	55.32%	33.57%	1.65%	9.01%
43	4.661	266	2.77E-01	0.28%	77.96%	14.73%	1.52%	5.51%
44	4.684	265	1.01E-01	0.29%	81.31%	14.21%	1.51%	2.69%
45	4.703	264	6.20E-02	0.23%	3.93%	11.17%	0.41%	84.26%
46	4.727	262	2.00E-01	1.57%	23.32%	64.59%	0.40%	10.13%
47	4.737	262	8.14E-01	1.21%	32.99%	55.28%	0.71%	9.81%
48	4.756	261	5.64E-01	1.28%	22.81%	71.59%	0.47%	3.85%
49	4.770	260	1.40E-02	0.11%	3.67%	7.17%	0.19%	88.87%
50	4.777	260	1.34E-01	0.96%	23.88%	65.68%	0.47%	9.02%

51	4.910	253	7.00E-03	8.69%	12.34%	64.49%	2.99%	11.50%
52	5.015	247	5.00E-03	8.89%	11.87%	65.14%	2.95%	11.15%
53	5.123	242	1.00E-03	1.01%	6.54%	86.60%	0.14%	5.72%
54	5.194	239	0.00E+00	0.07%	7.09%	87.05%	0.04%	5.75%
55	5.252	236	1.00E-03	0.20%	13.67%	72.53%	0.07%	13.52%
56	5.340	232	1.00E-03	1.16%	13.92%	71.75%	0.32%	12.85%
57	5.360	231	0.00E+00	0.25%	12.93%	73.88%	0.07%	12.87%
58	5.364	231	5.00E-03	0.86%	7.00%	84.34%	0.15%	7.66%
59	5.372	231	1.70E-02	0.20%	6.80%	86.60%	0.05%	6.35%
60	5.392	230	6.00E-03	0.36%	14.44%	72.33%	0.12%	12.75%
61	5.398	230	5.00E-03	1.20%	21.41%	68.95%	0.53%	7.92%
62	5.408	229	8.00E-03	0.41%	30.60%	63.33%	0.82%	4.85%
63	5.419	229	1.60E-02	0.40%	39.11%	54.06%	1.06%	5.36%
64	5.435	228	8.30E-02	1.22%	23.48%	60.47%	0.58%	14.25%
65	5.443	228	3.82E-01	0.10%	38.21%	7.45%	1.56%	52.68%
66	5.463	227	1.56E-01	0.35%	63.88%	15.21%	1.90%	18.66%
67	5.467	227	4.56E-01	0.24%	60.08%	8.01%	1.68%	29.98%
68	5.494	226	8.30E-02	0.14%	33.84%	5.95%	1.56%	58.51%
69	5.494	226	9.00E-03	0.34%	15.31%	71.53%	0.16%	12.68%
70	5.516	225	6.70E-02	0.19%	55.99%	7.27%	1.26%	35.29%
71	5.583	222	5.10E-02	0.46%	73.41%	9.74%	2.05%	14.34%
72	5.622	221	2.33E-01	0.37%	84.95%	6.02%	1.59%	7.07%
73	5.665	219	1.00E-02	10.30%	7.49%	75.78%	1.29%	5.13%
74	5.683	218	8.50E-02	0.55%	74.59%	14.00%	1.78%	9.09%
75	5.702	217	1.18E-01	0.34%	75.80%	14.02%	1.42%	8.42%
76	5.713	217	1.00E-03	1.01%	17.42%	68.22%	0.34%	13.02%
77	5.749	216	3.00E-03	0.48%	42.66%	42.99%	0.56%	13.32%
78	5.756	215	2.70E-02	0.50%	41.28%	38.44%	0.89%	18.89%
79	5.768	215	6.00E-03	0.12%	58.24%	15.30%	1.11%	25.22%
80	5.788	214	1.10E-02	0.17%	7.40%	5.78%	1.68%	84.97%

Comment about the so called “ π - π ” transition at 250 nm: this band corresponds to the overlay of several transitions: a first set, centered at 270 nm, is due to no less than four primarily LC-centered transitions ($S_0 \rightarrow S_{41}$ (271 nm), $S_0 \rightarrow S_{42}$ (270 nm), $S_0 \rightarrow S_{43}$ (266 nm) and $S_0 \rightarrow S_{44}$ (265 nm)), which account for the experimental shoulder around 290 nm. The second set, centered at 260 nm, is composed of $S_0 \rightarrow S_{46}$ (262 nm), $S_0 \rightarrow S_{47}$ (262 nm), $S_0 \rightarrow S_{48}$ (261 nm) and $S_0 \rightarrow S_{50}$ (260 nm), which are primarily MLCT states. We thus underline here the complexity of the observed transitions in the UV part of the spectra.

Table ST3. Emission (E_{em}), distortion (E_{dist}) and stabilization (E_{stab}) energies in eV, emission wavelength in nm (λ_{em}) and oscillator strength (f_{osc}) of the lowest S_1 and T_1 states for $[Cu(dipp)_2]^+$.

Structure	$[Cu(dipp)_2]^+$	
	S1A	T1A
E_{em}	1.631	1.356
λ_{em}	760	914
E_{dist}	0.441	0.442
E_{stab}	2.072	1.798
ΔE_{ST}		0.336
SOC		56.8

Table ST4. Bond lengths and angles of interest for the oxidized complex $[Cu(L1)_2]^{2+}$ (**Cu1**), $[Cu(dipp)_2]^{2+}$ and $[Cu(dtbp)_2]^{2+}$ computed with GAUSSIAN. Illustration of the phen-Cu-phen angle, defined by the angle between segments $(C\alpha-X)_{phenA}$ and $(C\alpha-X)_{phenB}$ (X = center of the phenyl ring).

Parameter	$[Cu(dipp)_2]^{charge}$		$[Cu(L1)_2]^{charge}$		$[Cu(dtbp)_2]^{charge}$	
	+	2+	+	2+	+	2+
Charge	+	2+	+	2+	+	2+
Cu-N1A	2.070	2.017	2.052	2.102	2.132	2.012
Cu-N2A	2.070	2.017	2.135	1.994	2.154	2.166
Cu-N1B	2.070	2.018	2.035	2.083	2.133	2.012
Cu-N2B	2.070	2.018	2.164	1.993	2.153	2.166
N1B-Cu-N2B	82.38	83.98	83.50	84.61	83.63	84.76
N1B-Cu-N1A	124.50	111.78	110.42	102.38	123.24	116.69
N1B-Cu-N2A	124.50	137.14	121.79	111.69	122.84	116.43
N2B-Cu-N1A	124.50	137.14	121.79	112.69	125.56	140.28
N2B-Cu-N2A	124.50	111.78	137.49	154.21	123.32	116.69
N1A-Cu-N2A	82.38	84.06	83.50	84.15	83.62	84.77
X-Cu-X	180.0	180.0	160.4	148.6	172.0	163.8
$C\alpha-X-X-C\alpha$	90.0	70.3	89.9	86.0	88.9	82.0
τ_4	0.79	0.61	0.71	0.66	0.79	0.73

References

- (1) Dobson, J. F.; Green, B. E.; Healy, P. C.; Kennard, C. H. L.; Pakawatchai, C.; White, A. H. The stereochemistry of Bis(2,9-dimethyl-1,10-phenanthroline)copper(I) complexes: the crystal and molecular structures of Bis(2,9-dimethyl-1,10-phenanthroline)copper(I) bromide hydrate, Bis(4,4',6,6'-tetramethyl-2,2'-bipyridine)copper(I) chloride dihydrate, and Bis(2,9-dimethyl-1,10-phenanthroline)copper(I) nitrate dihydrate (a redetermination). *Australian Journal of Chemistry* **1984**, *37*, 649-659,
- (2) Smith, C. S.; Mann, K. R. Void Space Containing Crystalline Cu(I) Phenanthroline Complexes As Molecular Oxygen Sensors. *Chem. Mater.* **2009**, *21*, 5042-5049, 10.1021/cm901109n.
- (3) Gandhi, B. A.; Green, O.; Burstyn, J. N. Facile Oxidation-Based Synthesis of Sterically Encumbered Four-Coordinate Bis(2,9-di-tert-butyl-1,10-phenanthroline)copper(I) and Related Three-Coordinate Copper(I) Complexes. *Inorg. Chem.* **2007**, *46*, 3816-3825, 10.1021/ic0615224.